Journal of Energy Chemistry 26 (2017) 309–314

Contents lists available at ScienceDirect

Journal of Energy Chemistry

journal homepage: www.elsevier.com/locate/jechem

http://www.journals.elsevier.com/journal-of-energy-chemistry/

Stability of $Ag@SiO_2$ core–shell particles in conditions of photocatalytic overall water-splitting

Sun-Young Park, Kai Han, Devin B. O'Neill, Guido Mul*

PhotoCatalytic Synthesis Group, MESA+ Institute for Nanotechnology, University of Twente, P.O. Box 217, 7500 AE Enschede, Netherlands

ARTICLE INFO

Article history:
Received 28 September 2016
Revised 9 December 2016
Accepted 28 December 2016
Available online 1 February 2017

Keywords:
Photocatalysis
Photoelectrochemistry
Water-splitting
Plasmon
Stability
Ag
SiO_2
Core–Shell
WO_3
ZnO
Mechanism

ABSTRACT

Core–shell nanoparticles containing plasmonic metals (Ag or Au) have been frequently reported to enhance performance of photo-electrochemical (PEC) devices. However, the stability of these particles in water-splitting conditions is usually not addressed. In this study we demonstrate that $Ag@SiO_2$ core–shell particles are instable in the acidic conditions in which WO_3-based PEC cells typically operate, Ag in the core being prone to oxidation, even if the SiO_2 shell has a thickness in the order of 10 nm. This is evident from in situ voltammetry studies of several anode composites. Similar to the results of the PEC experiments, the $Ag@SiO_2$ core–shell particles are instable in slurry-based, Pt/ZnO induced photocatalytic water-splitting. This was evidenced by in situ photodeposition of Ag nanoparticles on the Pt-loaded ZnO catalyst, observed in TEM micrographs obtained after reaction. We explain the instability of $Ag@SiO_2$ by OH-radical induced oxidation of Ag, yielding dissolved Ag^+. Our results imply that a decrease in shell permeability for OH-radicals is necessary to obtain stable, Ag-based plasmonic entities in photo-electrochemical and photocatalytic water splitting.

1. Introduction

Photo-electro-chemical or photocatalytic solar water splitting is promising technology to produce hydrogen sustainably, without significant CO_2 emissions associated with e.g. methane steam reforming or coal gasification. Since the first demonstration of this concept in 1972 by Honda and Fujishima based on TiO_2 [1], researchers aimed to develop improved semiconductor materials which could be used as photo-electrodes or photocatalysts for such process [2]. Besides doping to induce visible light activity, and deposition of catalytic nanoparticles to improve conversion efficiency, a third approach to enhance performance of semiconductors in photon induced processes is by functionalization of the surface with plasmonic nanoparticles [3–5]. Visible light photons then induce plasmonic resonance, thereby significantly stimulating/enhancing photocatalytic activity of the semiconductor [6]. Generally, metal nanoparticles are positioned in direct contact with the semiconductor to induce such plasmonic effects. A drawback of such configuration is that adverse recombination of electrons and holes at the metal/semiconductor interface might occur, or alternatively metal corrosion/oxidation induced by the electrolyte, eventually extinguishing the plasmonic enhancement.

To resolve these issues, and in particular metal corrosion, utilization of core–shell particles, preventing direct contact of the metal with the electrolyte and semiconductors used in photocatalysis and PEC cell configurations, has been demonstrated promising. Several reviews and excellent papers have appeared recently, addressing the synthesis and use of core–shell particles in heterogeneous catalysis [7–9], including core/yolk–shell nanocatalysts [10], or in energy applications [11,12]. Regarding photon induced processes, Thomann et al. convincingly showed plasmonic enhancement of Fe_2O_3 with $Au@SiO_2$ core–shell particles in water splitting applications [13], and Abdi et al. explored plasmonic enhancement by $Ag@SiO_2$ core–shell particles in contact with a $BiVO_4$-based photoanode [5]. Although Thomann et al. imply stability issues might be present, since the integrity of the shell might be affected by deformation as a result of thermal processing, the stability against oxidation of Ag in water splitting conditions, when present in core shell particles, has not been extensively addressed.

Herein, we explore the stability of $Ag@SiO_2$ core–shell particles in two relevant water splitting applications: (1) in a photo-electrochemical cell in contact with WO_3 as active component for water oxidation, and (2) in a physical mixture with Pt-loaded ZnO catalysts contained in a photocatalytic slurry reactor. We will

* Corresponding author.
E-mail address: G.Mul@utwente.nl (G. Mul).

http://dx.doi.org/10.1016/j.jechem.2016.12.010

demonstrate by electrochemical and electron microscopy analysis that significant oxidation of the silver core occurs in both configurations, despite the presence of the silica shell. The origin of this phenomenon is discussed.

2. Experimental

2.1. Synthesis and characterization of Ag@SiO_2 nanoparticles

Ag@SiO_2 core–shell nanoparticles were synthesized using a sol–gel method. A typical preparation procedure is as follows [14]. A 500 mL beaker was filled with 180 mL of aqueous solution including 0.145 g of CTAB under vigorous magnetic stirring. 10 mL of an aqueous solution of 0.1 M silver nitrate was added to this solution. 20 mL of 0.1 M ascorbic acid in aqueous solution was subsequently drop-wise added in a period of approximately 5 min. Afterwards, the mixture was stirred for 10 min, and 0.1 M sodium hydroxide was added to accelerate the chemical reaction, and to adjust the pH of the mixed solution to about 6.6. Subsequently, 50 mL of ethanol and 1 mL of TEOS were added to the silver colloid suspension, to create the silica shell. The solution was stirred for three more hours at room temperature. The thus synthesized Ag@SiO_2 core–shell particles were separated from the solution by a centrifuge, and dried in an oven at 80 °C in air, yielding a yellowish powder.

2.2. Preparation of WO_3 films on FTO glass

The preparation of the WO_3 photo-anode was performed as follows. First a WO_3 precursor solution was prepared, by dissolving 1.14 g of dark-blue WCl_6 (Sigma Aldrich) in 20 mL of ethanol in an inert atmosphere. It took several days to dissolve the WCl_6 salt accompanied by the disappearance of the original blue color, finally resulting in a transparent colorless liquid. The possible reaction path for the dissolution of WCl_6 in ethanol is described elsewhere [15]. For the preparation of the WO_3 film, the WO_3 precursor solution was spin-coated on fluorine-doped tin oxide glass (FTO; a thickness of ~600 nm, 16 Ω/cm^2) at 600 rpm for 30 s. After coating, the glass was heated on a hot plate at 100 °C for 1 min, and cooled. This process was repeated three consecutive times. Finally the samples were heated in a calcination oven at 500 °C (10 °C/min) for 2 h in static air. A SEM image of the resulting film is displayed in the supporting information (Fig. S1), demonstrating the WO_3 film is porous and has a thickness of ~300 nm.

2.3. Preparation of Ag@SiO_2 core–shell particles solution and coating

Several photo-anode configurations were prepared. For the preparation of an 'on top' configuration, an ethanol suspension containing Ag@SiO_2 core–shell particles (2 mg/4 mL) was treated for 30 min in an ultrasonic bath. Then 100 μL of such prepared suspension was spin coated on the pre-prepared WO_3 film at 1000 rpm for 40 s. After spin coating, the glass was heated on a hot plate to 100 °C for 1 min. This process was repeated consecutively to create a homogeneous layer of Ag@SiO_2 core–shell particles. For the preparation of an 'enclosed' configuration, a distilled water suspension containing Ag@SiO_2 core–shell particles (2 mg/4 mL) was treated for 30 min in an ultrasonic bath. Then 100 μL of the prepared suspension was spin coated on FTO glass at 2000 rpm for 40 s. After coating, the glass was heated on a hot plate at 100 °C for 1 min. This process was repeated consecutively to create a homogeneous layer of Ag@SiO_2 core–shell particles. Subsequently WO_3 was deposited according to the previously described procedure (Section 2.2).

2.4. Characterization of the PEC cell in water splitting

The photoelectrochemical anodic properties of the WO_3/Ag@SiO_2 core–shell particle composites were determined in an aqueous electrolyte solution containing 0.1 M of sodium sulfate (pH ~3.5). The potential of the working electrode was controlled by a potentiostat (VERSASTAT 4, Princeton applied research). In the three-electrode measurements, a Pt wire and an Ag/AgCl electrode (3 M NaCl, BASi) were used as the counter and reference electrode, respectively. The photoactive area was defined by an o-ring positioned in front of the WO_3 anode, being 2.54 cm^2 [16]. Photocurrents were measured under illumination of an AM 1.5 solar simulator (100 mW/cm^2), with a 300 Xe lamp and air mass 1.5 global filter. The intensity of the simulated sunlight was calibrated using a standard reference Si solar cell.

2.5. Photo-deposition of Pt nanoparticles on ZnO

1 g of ZnO (Sigma Aldrich) suspended in Milli-Q water (40 mL) was mixed with 7 mL of 0.0019 M H_2PtCl_6•$6H_2O$ solution in a quartz glass beaker for 30 min in dark conditions. The beaker was capped by a quartz glass plate to prevent evaporation, and covered by aluminum foil. 3 mL of methanol was added to the thus prepared solution as sacrificial agent, followed directly by illumination using UV light (18 W TL-D Blacklight Blue, Philips) for 1 h. The total light intensity was 3.21 mW/cm^2 with the wavelength ranging from 360 to 380 nm. The thus synthesized Pt-loaded ZnO was centrifuged and washed 3 times by Milli-Q water and then dried in an oven at 80 °C under atmospheric conditions.

2.6. Characterization of photocatalyst activity by gas chromatography

H_2 evolution was measured for the Pt-loaded ZnO photocatalyst in a continuously stirred tank reactor (CSTR) connected to a gas chromatograph (CompactGC Interscience), equipped with a pulsed discharge detector. 25 mg of photocatalyst was dispersed in 25 mL of 0.01 M K_2SO_4 (pH ~7.7) within an optical glass cuvette of 50 mL, used as CSTR. After removing air from the reactor by continuous purging with purified He, the suspension was illuminated by a solar simulator at 100 mW/cm^2 (Abet Technologies, Inc., 150 W ozone free arc lamp). The amount of H_2 evolution was continuously measured using Helium as purge gas (10 mL/min). To determine the effect of Ag@SiO_2 core–shell particle on the water splitting efficiency, Ag@SiO_2 core–shell particles were added after 4 h of illumination of the Pt-loaded ZnO sample in suspension. Before introduction of the Ag@SiO_2 core–shell particles, the reactor was purged to remove H_2 from the reactor in dark conditions.

2.7. Analysis of photo-electrode

The various photo-anodes and photocatalyst samples were analyzed using field emission scanning electron microscope (FE-SEM, Zeiss LEO 1550), Transmission electron microscopy (HR-TEM, FEI Instruments), X-ray photoelectron spectroscopy (XPS, Quantera SXM from Physical Electronics), X-ray diffraction (XRD, Bruker D2 phaser), and inductively coupled plasma atomic emission spectroscopy (ICP-AES, Varian Liberty II, Sequential ICP-AES). UV/vis spectroscopy was performed in transmission mode, using a Thermo Scientific Evolution 600 spectrometer and Millipore water as reference. Pt and Ag particle sizes, oxidation states, crystallinity of the semiconductors and Pt loading, were thus obtained, respectively.

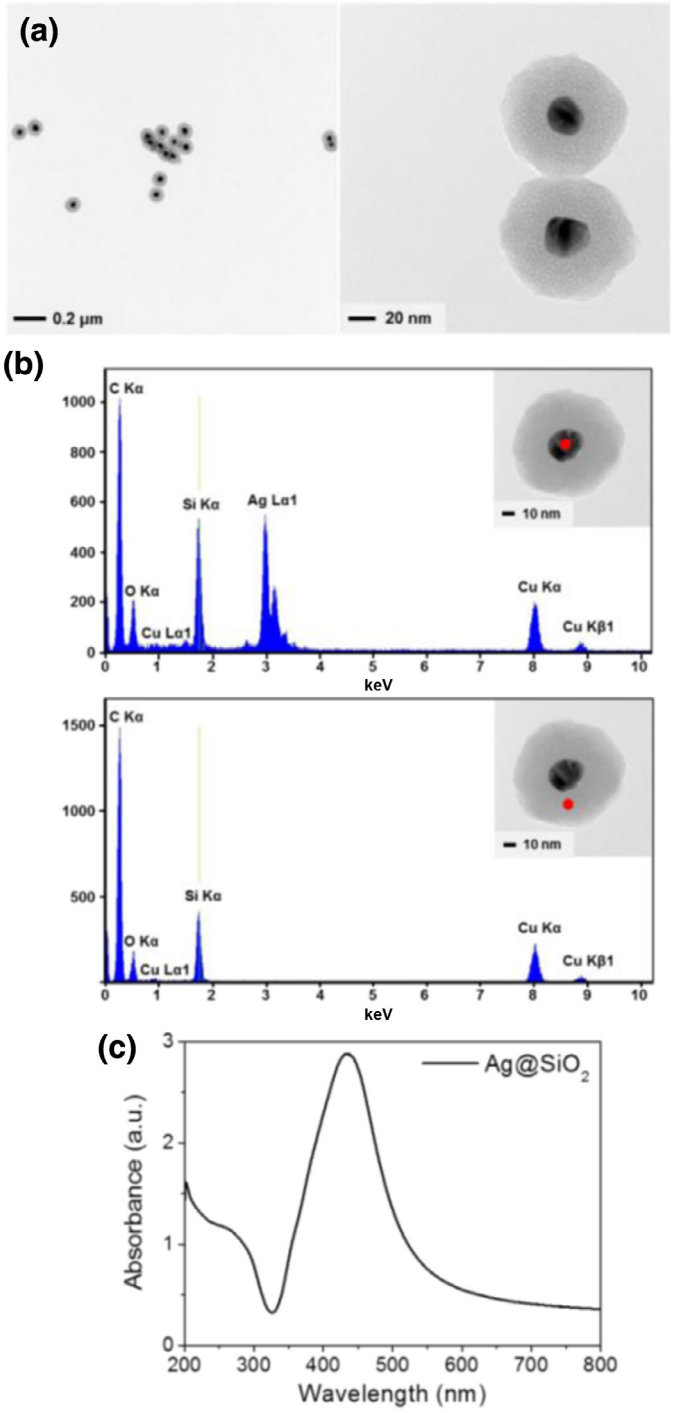

Fig. 1. Characterization of the Ag@SiO_2 core–shell particles. (a) TEM micrographs (b) EDX spectra, and (c) the UV–vis spectrum showing the plasmon absorption band. The core–shell structure is confirmed, and the plasmon absorption at around 420 nm in agreement with literature.

3. Results

3.1. Catalyst characterization

Fig. 1(a) shows the transmission electron microscopy (TEM) images of the as synthesized Ag@SiO_2 core–shell particles. Spherical nanoparticles with a diameter of ~20 nm of the Ag core, and a shell thickness of SiO_2 of ~20 nm, were obtained. The energy-dispersive X-ray spectroscopy (EDX) spectra of the core and the shell of the Ag@SiO_2 core–shell particles are shown in Fig. 1(b), confirming the core consists of Ag, and the shell of Si. The Cu signature is due to the grid applied for the TEM analysis. A UV–vis absorption spectrum of the Ag@SiO_2 core–shell particles, when present in suspension in distilled water, is shown in Fig. 1(c). The maximum absorption peak is located around 420 nm, in agreement with literature [6].

To determine if plasmonic enhancement of the as-prepared Ag@SiO_2 core–shell particles was feasible, we used Raman spectroscopy (Fig. S2) to evaluate intensity differences in WO_3 induced Raman lines. The features at 710 and 805 cm^{-1} can be attributed to W–O–W stretching modes of the WO_3 film [17]. The presence of bare Ag nanoparticles results in higher relative Raman intensities of WO_3, as compared to WO_3–FTO. The presence of Ag@SiO_2 core–shell particles (WO_3–Ag@SiO_2–FTO layers) still showed enhancement, albeit significantly less, indicating the shell thickness, above which plasmonic features are quenched, was reached.

3.2. Characterization by photo-electrochemical analysis

Fig. 2(a) shows the current density for an enclosed configuration in which the Ag@SiO_2 core–shell particles are positioned in between the FTO-glass electrode and the WO_3 film. We controlled the amount of Ag@SiO_2 core–shell particles by increasing the number of spin coating cycles from 1 to 3, before deposition of WO_3. The effect of the Ag@SiO_2 core–shell particles on photocurrent efficiency is negative, even after a single spin coating cycle. As indicated in the cartoon, the *negative* effect of the presence of Ag@SiO_2 is likely explained by a reduction in effective contact between the WO_3 film and the FTO substrate, more dominant for a thicker than a thinner film of the Ag@SiO_2 particles. This might introduce significant resistances for electron flow from WO_3 into FTO. Apparently, this negative effect is not (over)compensated by plasmonic enhancement. Fig. 2(b) shows the dark current of the applied electrode configurations, clearly demonstrating an anodic peak in the voltage range of 0.65 till 0.8 V vs. RHE.

To further analyze this anodic peak, dark scan curves of FTO-glass, bare SiO_2 on FTO-glass, bare Ag nanoparticles on FTO-glass, and Ag@SiO_2 core–shell particles on FTO- glass, are compared in Fig. 3. The Ag@SiO_2 core–shell particles show a similar anodic current peak to the Ag nanoparticles without a shell, albeit of much lower intensity as evident from the magnified view (Fig. 3(b)). The oxidation current can be assigned to oxidation and dissolution of Ag:

$$Ag \rightarrow Ag^{+} + e \quad (1)$$

Ag is thus instable at the applied (and generated) oxidation potential over a broad range of pH values, [18] and Ag appears only partly stabilized by the silica shell. We therefore conclude that plasmonic effects will be diminished at potentials lower than the potential required for significant water oxidation induced by WO_3.

LSV curves of WO_3 anodes with Ag@SiO_2 core–shell particles deposited on top of WO_3, are presented in Fig. S3. The presence of Ag@SiO_2 again decreases the photocatalytic performance of WO_3 in conversion of water to O_2. We propose light scattering and shielding explain the negative effect of Ag@SiO_2 in this electrode configuration, in particular when front illumination is applied. We also anticipate oxidation of Ag is again occurring, preventing plasmonic enhancement. If so, intimate contact between the Ag@SiO_2 particles and the photo-electrode is apparently unnecessary to induce oxidation. To verify this hypothesis, we evaluated the stability of Ag@SiO_2 in the presence of platinized ZnO when illuminated in water-splitting conditions.

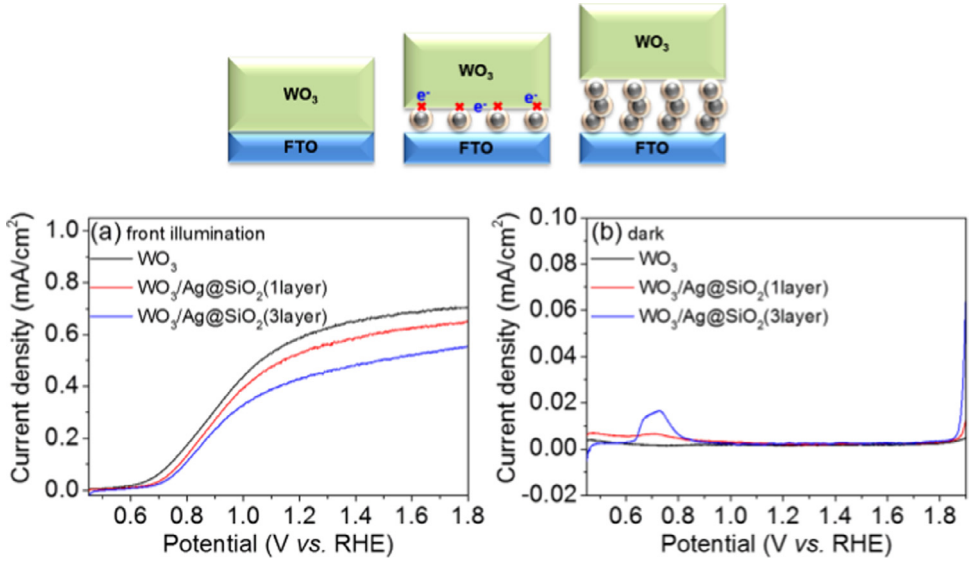

Fig. 2. LSV curves of an unmodified WO_3 electrode, and an electrode containing $Ag@SiO_2$ core–shell particles between the WO_3 film and FTO-glass under (a) front-side illumination and (b) in dark conditions.

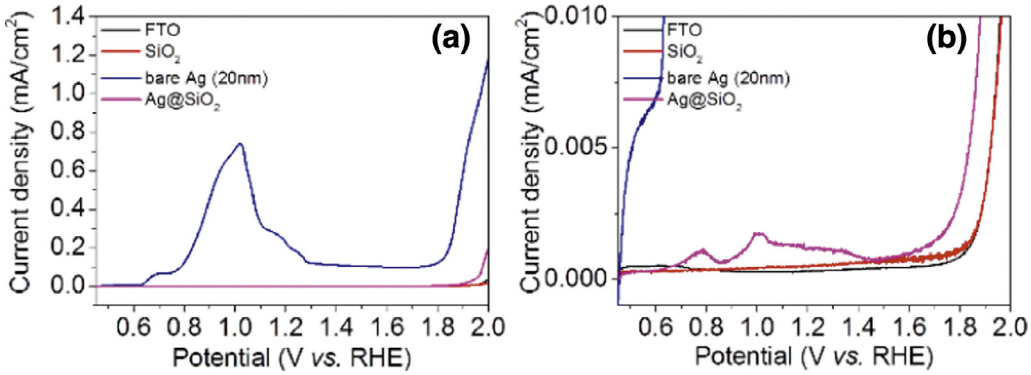

Fig. 3. (a) Dark scan curves of FTO glass, SiO_2 on FTO-glass, Ag nanoparticles on FTO-glass, and $Ag@SiO_2$ core–shell particles on FTO-glass. (b) Magnified view of the same experiment.

3.3. Stability of $Ag@SiO_2$ in a photocatalytic slurry reactor

Gas chromatography measurements of hydrogen and oxygen evolution induced by illuminated Pt-loaded ZnO in the absence or presence of $Ag@SiO_2$ core–shell particles are shown in Fig. 4. Fig. 4 clearly shows that ZnO requires Pt nanoparticles to induce the formation of hydrogen. The Pt-loaded ZnO sample produces approximately ~400 ppb H_2 (in 10 mL/min He flow) under 1 sun illumination. The presence of $Ag@SiO_2$ core–shell particles enhances H_2 evolution rate to some extent, likely due to light-scattering effects, contrary to the electrode configuration now favoring a more homogeneous illumination of the volume of the slurry reactor. In the presence of 10 wt% of the $Ag@SiO_2$ particles (on the basis of Pt/ZnO), the activity of the Pt/ZnO catalyst is in the order of 0.58 $\mu mol_{H2}/(g{\cdot}h)$.

We could not detect the formation of O_2, even though our pulsed-discharge-detector has sufficient sensitivity for the O_2 quantities expected on the basis of the quantities of H_2. We speculate, that the following alternative reactions for water oxidation might be relevant [19].

(1) Oxidation of carbon contaminants to CO or CO_2 by (activated) oxygen (reaction (2)).

$$\text{“C” on the ZnO surface} + O_2 \rightarrow CO + CO_2 \quad (2)$$

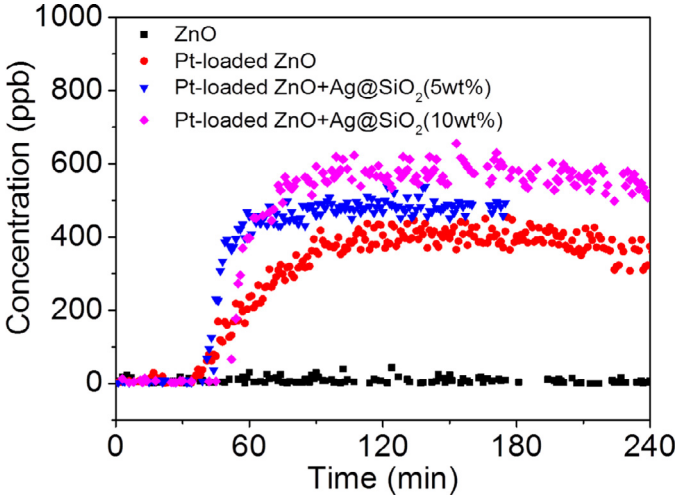

Fig. 4. Gas chromatography measurement of water splitting induced by Pt-loaded ZnO in the absence or presence of $Ag@SiO_2$ core–shell particles. Only hydrogen was detected in significant amounts.

Unfortunately our GC configuration was not able to measure CO_2 during the reaction, but the formation of CO can be excluded.

Carbon contaminants are well-known to be present on semiconductor surfaces [20].

(2) Photo-excited holes react with water to produce hydroxyl radicals (reaction (3)), followed by formation of hydrogen peroxide (reaction (4)), rather than oxygen.

$$4h^+ \text{ (from ZnO)} + 4H_2O \rightarrow 4OH\bullet + 4H^+ \quad (3)$$

$$4\ OH\bullet \rightarrow 2H_2O_2 \quad (4)$$

Reaction (3) is also very likely to occur, as we will further address in Section 4.2.

Several samples were analyzed before and after the water splitting reaction by TEM (Fig. 5). ZnO used in the present study consists of plate-like, well-defined crystals, with sizes in range of 100 to a few 100 s of nanometers (Fig. 5(a)). Fig. 5(b) shows the sample obtained after photodeposition of Pt nanoparticles. The integrity of the ZnO crystals is not significantly changed by the photodeposition procedure, as confirmed by XRD data shown in Fig. S4, while small homogeneously distributed Pt nanoparticles can be observed. Using the program image J (see supplementary information Fig. S5), we determined an average Pt-particle size in the order of 1.94 nm ± 0.7 nm. ICP-AES confirmed that photo-deposition of Pt on ZnO occurred with an efficiency of 99.5%. Reduction of the Pt-precursor was not fully complete, since the presence of some Pt(II)O was identified by XPS analysis (Fig. S6).

$Ag@SiO_2$ core–shell particles are also clearly visible in the images of the Pt-loaded ZnO (Fig. 5(c)). Fig. 5(d) shows images taken after the photocatalytic reaction. Several remarkable observations can be made. First, the image shows a $Ag@SiO_2$ core–shell particle in which the Ag core has clearly shrunk, leaving a void between the shell and the (smaller) Ag particle. Second, relatively large Ag metal particles appear to have deposited on the ZnO crystals, which can be clearly discerned from the Pt particles by EDX as shown in Fig. S7. The Pt particles did not significantly change in morphology, but were determined by XPS analysis (Fig. S8) to be fully reduced to the metallic state (Pt^0), on the basis of the peak position at 71.0 eV. In situ reduction of PtO_x upon illumination of ZnO is entirely feasible, and might occur as schematically illustrated in Fig. 6. Conversion of oxidic Pt is in agreement with the transient in hydrogen production rate, which increases in the initial hour of the experiment.

4. Discussion

4.1. Stability of $Ag@SiO_2$ in photo-electro-chemical water splitting conditions

Various studies have demonstrated that plasmonic enhancement by Au or Ag nanoparticles is feasible in photo-electrochemical applications. A very illustrative study has been reported by Abdi et al. who explored the application of $Ag@SiO_2$ core–shell nanoparticles on the surface of $BiVO_4$ to improve the absorption in $BiVO_4$ [5]. Contrary to our data for WO_3, Abdi et al. found enhancement in photocurrent, when $Ag@SiO_2$ was in contact with $BiVO_4$, which they tentatively explain by improvement of water oxidation kinetics due to catalytic activity of $Ag@SiO_2$ nanoparticles. They arrived at this explanation on the basis of a similar experiment as shown in Fig. 3, in which they also observed an electrochemical response. Instability of the $Ag@SiO_2$ particles in photo-electrochemical conditions was, however, not considered. Alternatively to the explanation of Abdi et al., we propose our electrochemical response in Fig. 3 is due to the (sacrificial) oxidation of the Ag core, which we presume in photo-electrochemical conditions is predominantly electrochemical (see reaction (1)).

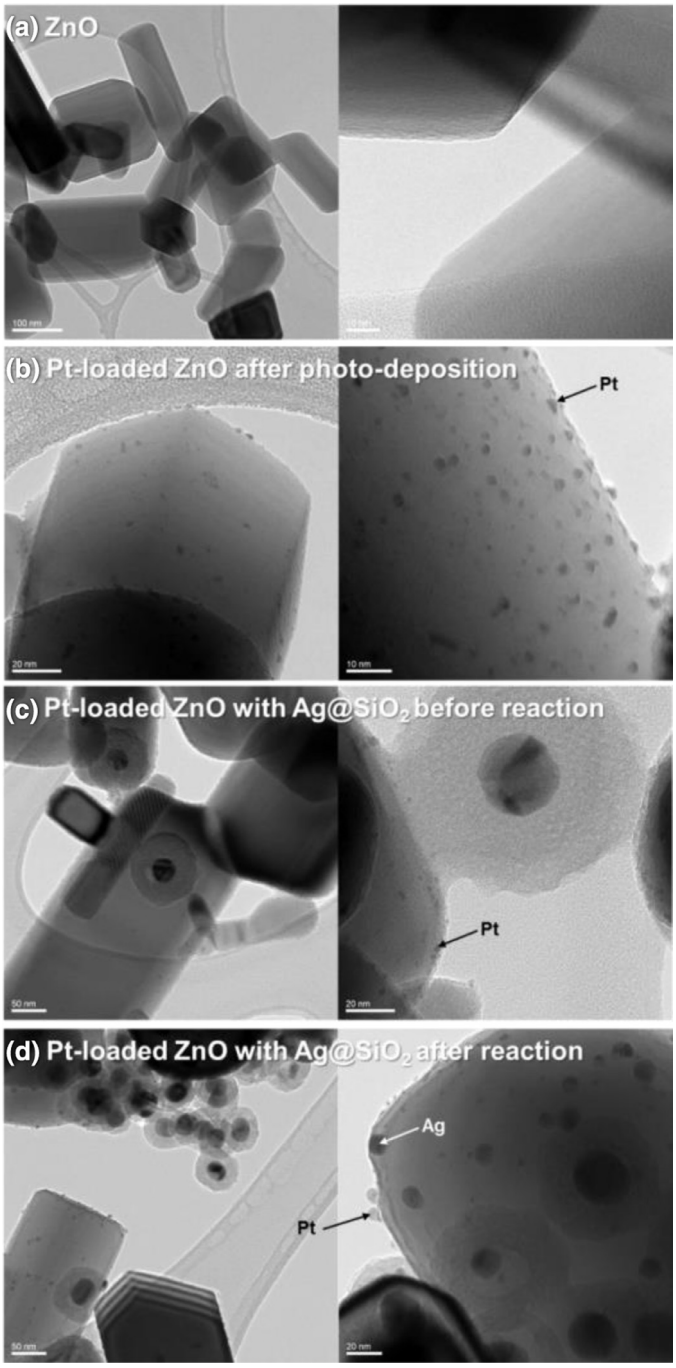

Fig. 5. TEM images of (a) ZnO (scale-bar 100 nm and 10 nm), (b) Platinized ZnO after photo-deposition (scale-bar 20 nm and 10 nm), (c) a physical mixture of platinized ZnO with $Ag@SiO_2$ before the water splitting reaction (scale-bar 50 nm and 20 nm), and (d) a physical mixture of platinized ZnO with $Ag@SiO_2$ after the water splitting reaction (scale-bar 50 nm and 20 nm).

Based on the photocatalysis data, there is additional, alternative chemistry for oxidation of Ag, which will be discussed as follows.

4.2. Stability of $Ag@SiO_2$ in photo-catalytic water splitting conditions

To the best of our knowledge, there is no study in the literature that has addressed the (in)stability of $Ag@SiO_2$ core shell particles in photocatalytic water-splitting applications. To explain our phenomena (Fig. 5), we propose the following reaction sequence.

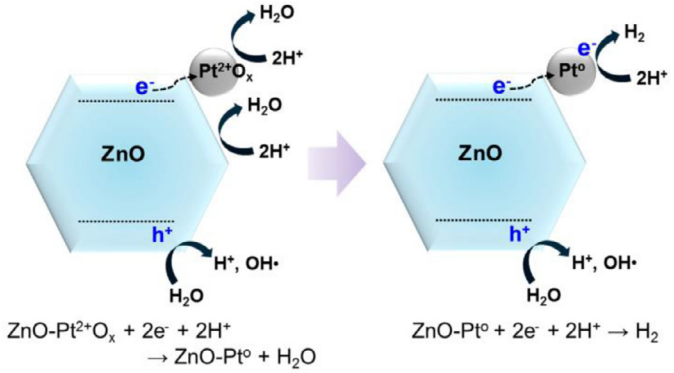

Fig. 6. Illustration of the processes initially occurring upon illumination of Pt/ZnO in water-splitting conditions.

First, photo-excited ZnO induces the formation of hydroxyl radicals according to reaction (3). Recent studies have demonstrated that these radicals can dissolve in water. These are apparently also capable of penetrating the porous SiO_2 shell, and to induce oxidation of Ag to Ag^+ according to reaction (5). Then we assume Ag^+ to diffuse out of the shell into solution, after which Ag^+ reacts with the photo-excited electron from ZnO to create Ag nanoparticles (reaction (6)), similar to a photo-deposition process.

$$OH\bullet + Ag\ (\text{core of } Ag@SiO_2) \rightarrow Ag^+ + OH^- \quad (5)$$

$$Ag^+\ (\text{in solution}) + e^- \rightarrow Ag\ (\text{on ZnO}) \quad (6)$$

In fact, the observation of photodeposited Ag particles on ZnO is evidence that Ag^+ ions are transported through the shell-wall, thus leaching into solution. Re-deposition of Ag on the ZnO surface was that effective, that Ag^+ concentrations were below the detection limit of the ICP-AES instrument. Corroborating the porosity of the silica shell, are the results reported by Suryanarayanan et al. [21]. They showed the Ag core of $Ag@SiO_2$ core–shell particles can be oxidized into silver ions by reaction with halocarbons. Loss of the integrity of the shell by deformation as a result of thermal processing, as proposed by Thomann et al. [7], might increase the porosity and exposure of Ag to the electrolyte solution and dissolved hydroxyl radicals therein. Our results imply that Ag nanoparticles need to be covered with a dense, non-porous SiO_2 shell, to ensure stability in photo-electrochemical and photocatalytic water splitting conditions. CTAB, used in this study to prepare the silica shell, has been used to produce (meso)porous films of silica, including hexagonal porous films [22]. Films of higher density can be synthesized through the use of a silane coupling agent (such as (3-aminopropyl)trimethoxysilane) which can replace CTAB yielding a monolayer of dense SiO_2 [23,24], or by growth off of a polyvinylpyrrolidone (PVP) surface [25]. Use of these methods should allow for the formation of a thinner and denser silica film. The use of a silane coupling agent may not prevent all access to the surface, as Suryanarayanan et al. [15] observed degradation of Ag particles in SiO_2 shells grown on APTMS over 14 h of cyclic voltammetry. Future study in our laboratory will focus on synthesis methods providing dense silica shells, to enhance stability of the Ag in $Ag@SiO_2$ particles. We will also address the efficient removal of carbon residues used in the various synthesis procedures.

5. Conclusions

In summary, we have analyzed the performance of $Ag@SiO_2$ core–shell particles in WO_3-based photo-electrochemical water splitting and in Pt/ZnO based photocatalytic water-splitting. Electrochemical oxidation of the Ag core was demonstrated to occur at potentials lower than required for WO_3 induced water oxidation, explaining the absence of plasmonic enhancement in photocurrent. Based on the TEM images obtained after Pt/ZnO based photocatalytic water splitting, we propose oxidation of Ag by OH-radicals is also feasible, resulting in hollow $Ag@SiO_2$ particles, dissolution of Ag^+, and (photo)deposition of Ag on ZnO. Our results thus suggest that the shell morphology of $Ag@SiO_2$ should be optimized to (i) minimize electrical contact of Ag with a photoanode, (ii) to prevent OH-radical based oxidation and dissolution of the Ag core, and (iii) to preserve plasmonic enhancement in photo-electrochemical and photocatalytic water splitting.

Acknowledgments

This work is part of the research programme of the Foundation for Fundamental Research on Matter (FOM, project 10TBSC07-1), which is part of the Netherlands Organisation for Scientific Research (NWO).

Supplementary materials

Supplementary material associated with this article can be found, in the online version, at doi:10.1016/j.jechem.2016.12.010.

References

[1] A. Fujishima, K. Honda, Nature 238 (1972) 37–38.
[2] A. Kudo, Y. Miseki, Chem. Soc. Rev. 38 (2009) 253–278.
[3] W. Hou, S.B. Cronin, Adv. Funct. Mater. 23 (2013) 1612–1619.
[4] S.C. Warren, E. Thimsen, Energy Environ. Sci. 5 (2012) 5133–5146.
[5] F.F. Abdi, A. Dabirian, B. Dam, R. van de Krol, Phys. Chem. Chem. Phys. 16 (2014) 15272–15277.
[6] S. Linic, P. Christopher, D.B. Ingram, Nat. Mater. 10 (2011) 911–921.
[7] P.M. Arnal, M. Comotti, F. Schuth, Angew. Chem. Int. Ed. 45 (2006) 8224–8227.
[8] L. De Rogatis, M. Cargnello, V. Gombac, B. Lorenzut, T. Montini, P. Fornasiero, ChemSusChem 3 (2010) 24–42.
[9] S.H. Joo, J.Y. Park, C.K. Tsung, Y. Yamada, P.D. Yang, G.A. Somorjai, Nat. Mater. 8 (2009) 126–131.
[10] Z.W. Li, M. Li, Z.F. Bian, Y. Kathiraser, S. Kawi, Appl. Catal. B Environ. 188 (2016) 324–341.
[11] C. Galeano, J.C. Meier, V. Peinecke, H. Bongard, I. Katsounaros, A.A. Topalov, A.H. Lu, K.J.J. Mayrhofer, F. Schuth, J. Am. Chem. Soc. 134 (2012) 20457–20465.
[12] M.B. Gawande, A. Goswami, T. Asefa, H.Z. Guo, A.V. Biradar, D.L. Peng, R. Zboril, R.S. Varma, Chem. Soc. Rev. 44 (2015) 7540–7590.
[13] I. Thomann, B.A. Pinaud, Z.B. Chen, B.M. Clemens, T.F. Jaramillo, M.L. Brongersma, Nano Lett. 11 (2011) 3440–3446.
[14] K. Xu, J.-X. Wang, X.-L. Kang, J.-F. Chen, Mater. Lett. 63 (2009) 31–33.
[15] B.W. Mwakikunga, A. Forbes, E. Sideras-Haddad, M. Scriba, E. Manikandan, Nanoscale Res. Lett. 5 (2009) 389–397.
[16] S.Y. Park, E.M. Hong, D.C. Lim, J.Y. Lee, G. Mul, J. Electrochem. Soc 163 (2016) H105–H109.
[17] L. Xu, M.-L. Yin, S. Liu, Sci. Rep. 4 (2014).
[18] F.W. Campbell, R.G. Compton, Anal. Bioanal. Chem. 396 (2010) 241–259.
[19] T. Abe, E. Suzuki, K. Nagoshi, K. Miyashita, M. Kaneko, J. Phys. Chem. B 103 (1999) 1119–1123.
[20] C.C. Yang, Y.H. Yu, B. van der Linden, J.C.S. Wu, G. Mul, J. Am. Chem. Soc. 132 (2010) 8398–8406.
[21] V. Suryanarayanan, A.S. Nair, R.T. Tom, T. Pradeep, J. Mater. Chem. 14 (2004) 2661–2666.
[22] M. Klotz, A. Ayral, C. Guizard, L. Cot, J. Mater. Chem. 10 (2000) 663–669.
[23] V. Uzayisenga, X.D. Lin, L.M. Li, J.R. Anema, Z.L. Yang, Y.F. Huang, H.X. Lin, S.B. Li, J.F. Li, Z.Q. Tian, Langmuir 28 (2012) 9140–9146.
[24] L.M. Liz-Marzan, M. Giersig, P. Mulvaney, Langmuir 12 (1996) 4329–4335.
[25] J.P. Yang, F. Zhang, Y.R. Chen, S. Qian, P. Hu, W. Li, Y.H. Deng, Y. Fang, L. Han, M. Luqman, D.Y. Zhao, Chem. Commun. 47 (2011) 11618–11620.